PNAS RESEARCH ARTICLE | MICROBIOLOGY OPEN ACCESS

The Sde phosphoribosyl–linked ubiquitin transferases protect the *Legionella pneumophila* vacuole from degradation by the host

Seongok Kim[a] and Ralph R. Isberg[a,1]

Contributed by Ralph R. Isberg; received March 10, 2023; accepted July 5, 2023; reviewed by Jost Enninga and Zhaoqing Luo

Legionella pneumophila **grows intracellularly within the membrane-bound *Legionella*-containing vacuole (LCV) established by proteins translocated via the bacterial type IV secretion system (T4SS). The Sde family, one such group of translocated proteins, catalyzes phosphoribosyl–ubiquitin (pR-Ub) modification of target substrates. Mutational loss of the entire Sde family results in small defects in intracellular growth, making it difficult to identify a clear role for this posttranslational modification in supporting the intracellular lifestyle. Therefore, mutations that aggravate the loss of *sde* genes and caused intracellular growth defects were identified, providing a mechanistic connection between Sde function and vacuole biogenesis. These double mutants drove the formation of LCVs that showed vacuole disintegration within 2 h of bacterial contact. Sde proteins appeared critical for blocking access of membrane-disruptive early endosomal membrane material to the vacuole, as RNAi depletion of endosomal pathway components partially restored LCV integrity. The role of Sde proteins in preventing host degradation of the LCV was limited to the earliest stages of infection. The time that Sde proteins could prevent vacuole disruption, however, was extended by deletion of *sidJ*, which encodes a translocated protein that inactivates Sde protein active sites. These results indicate that Sde proteins act as temporally regulated vacuole guards during the establishment of the replication niche, possibly by constructing a physical barrier that blocks access of disruptive host compartments during the earliest steps of LCV biogenesis.**

Legionella | macrophage | intracellular growth | reticulon | vacuoles

Legionella pneumophila is an intravacuolar pathogen of amoebae that can cause pneumonic disease in susceptible human hosts (1, 2). As a causative agent of Legionnaires' disease, infection is driven by inhalation or aspiration of contaminated water, followed by bacterial growth within alveolar macrophages (3, 4). Failure to clear infection from the lungs in the immunocompromised patient results in life-threatening disease.

Successful intracellular growth in hosts depends on the establishment of the specialized *Legionella*-containing vacuolar (LCV). Upon internalization, more than 300 different effectors are translocated through the Icm/Dot type IV secretion system (T4SS) into host cells (5–9). The Icm/Dot translocated substrates (IDTS) hijack host-membrane trafficking pathways, redirecting components of the host cell secretory system to remodel the pathogen compartment into a replication-permissive LCV (10). Most notable is the ability of the LCV to avoid phagosome maturation as a consequence of association with the endoplasmic reticulum (ER), bypassing fusion with compartments that can lead to either microbial degradation or dissolution of the LCV membrane (10–14). Mutations in the Icm/Dot system prevent LCV formation and block intracellular growth, although deletions of single secreted effectors result in either small or undetectable intracellular replication defects. The inability to uncover intracellular growth defects from loss of single effectors is consistent with genetic redundancy, resulting from multiple substrates targeting a single host membrane–trafficking pathway or multiple host pathways working in parallel to support LCV biogenesis (6, 15).

The Sde family (*sdeA*, *sdeB*, *sdeC* and *sidE* in the Philadelphia 1 clinical isolate) is a group of homologous IDTS that contains an N-terminal deubiquitinase (DUB), a nucleotidase/phosphohydrolase (NP) domain, and a central mono-ADP-ribosyltransferase domain (mART). The mART domain ADPribosylates host ubiquitin (Ub) that, in turn, is used as a substrate for the NP domain to promote phosphoribosyl-linked Ub (pR-Ub) modification of target host proteins (16–23). One of the primary targets of the Sde family is host reticulon 4 (Rtn4) (19, 22, 24, 25). Phosphoribosyl-Ub modification of Rtn4 promotes endoplasmic reticulum (ER) rearrangements about the LCV within minutes of bacterial contact with host cells (22). Although the absence of Sde family proteins results

Significance

Maintaining replication compartment integrity is critical for growth of intravacuolar pathogens within host cells. By identifying genetically redundant pathways, *Legionella pneumophila* Sde proteins that promote phosphoribosyl-linked ubiquitination of target eukaryotic proteins are shown to be temporally regulated vacuole guards, preventing replication vacuole dissolution during early stages of infection. As targeting of reticulon four by these proteins leads to tubular endoplasmic reticulum aggregation, Sde proteins are likely to construct a barrier that blocks access of disruptive early endosomal compartments to the replication vacuole. Our study provides a framework for how vacuole guards function to support biogenesis of the *L. pneumophila* replicative niche.

Author affiliations: [a]Department of Molecular Biology and Microbiology, Tufts University School of Medicine, Boston, MA 02111

Author contributions: S.K. and R.R.I. designed research; S.K. performed research; S.K. and R.R.I. analyzed data; and S.K. and R.R.I. wrote the paper.

Reviewers: J.E., Institut Pasteur; and Z.L., The First Hospital of Jilin University.

The authors declare no competing interest.

[1]To whom correspondence may be addressed. Email: ralph.isberg@tufts.edu.

This article contains supporting information online at https://www.pnas.org/lookup/suppl/doi:10.1073/pnas.2303942120/-/DCSupplemental.

Published August 7, 2023.

in small intracellular growth defects in amoebal hosts (26), these defects are subtle during macrophage challenge, consistent with genetic redundancy. This argues that unidentified bacterial translocated effectors may compensate for loss of the Sde family by targeting parallel host pathways that support LCV biogenesis. Redundancy is likely to be limited to the earliest stages of infection, as other IDTS negatively regulate the function of the Sde family. For instance, the mART activity of Sde proteins is inactivated by SidJ, a meta-effector that glutamylates the Sde active site residue (26–29). Furthermore, pR-Ub modification of target proteins is reversed by a pair of pR-Ub-specific deubiquitinases, DupA/B, arguing for temporally limiting Sde family function (24, 25).

In this work, we identified proteins that may compensate for loss of Sde function. Chief among them is the T4SS substrate SdhA protein, which is required for maintaining membrane integrity of the LCV (30, 31). SdhA binds the OCRL phosphatase involved in the regulation of early and recycling endosomes, and likely diverts these disruptive compartments from interacting with the LCV (32–34). In the absence of SdhA, the bacteria are exposed to host cytosol and subjected to bacterial degradation by interferon-regulated proteins, leading to pyroptotic host cell death (35, 36). RNAi depletion of Rab5, Rab11 and Rab8, which are guanosine triphosphatases (GTPase) involved in regulating the endocytic and recycling endosome pathways, partially recovers loss of LCV integrity seen in the absence of SdhA, consistent with these compartments disrupting LCV integrity (37).

A second *L. pneumophila* translocated effector that interfaces with the retromer complex is RidL which binds to host VPS29, blocking the function of the retromer, which is critical for recycling cargo from endosomes to the trans-Golgi network and to the plasma membrane (38–40). Retrograde trafficking is thought to be blocked by RidL as a consequence of diverting the retromer to sites on the LCV (40), displacing components known to be required for GTP activation of the complex (41).

Using transposon sequencing (Tn-Seq) to unveil redundant effectors involved in LCV biogenesis, we found mutations in three genes (*sdhA*, *ridL,* and *legA3*) that aggravate loss of Sde family function. Given the known functions of these effectors, this work argues that Sde proteins act to catalyze formation of a temporally regulated physical barrier to protect the LCV from attack by host compartments that disrupt the membrane integrity of the replication niche.

Materials and Methods

Bacterial Strains, Cultures, Cells, and Growth Media. *L. pneumophila* strains were grown in liquid N-(2-acetamido)-2-aminoethanesulfonic acid (ACES)–buffered yeast extract (AYE) media or on solid charcoal–buffered yeast extract (CYE) media containing 0.4 *g*/l iron (III) nitrate, 0.135 *g*/mL cysteine, and 1% α-ketoglutaric acid. Then, 40 μg/mL kanamycin, 5% (vol/vol) sucrose, 1 mM IPTG or 5 μg/mL chloramphenicol were added when appropriate. *E. coli* strains were cultured in liquid LB or on solid LB plates supplemented with 50 μg/mL kanamycin or 12.5 μg/mL chloramphenicol when appropriate. Primary bone marrow-derived macrophages (BMDM) from AJ mice were prepared and cultured as described previously (13).

Construction of *L. pneumophila* Transposon Mutant Library. Electrocompetent (42) *L. pneumophila* Philadelphia-1 strains SK01(*sde*$^+$) and SK02 (Δ*sde*) were transformed with 75 ng pTO100*MmeI* (43), respectively, plated on CYE supplemented with kanamycin and sucrose, and incubated at 37 °C for 4 d. Multiple pools were made from each strain, each containing 50,000 to 80,000 colony forming units (CFUs), which were subsequently harvested and pooled into AYE containing 20% (vol/vol) glycerol. Bacterial suspensions were aliquoted at a concentration ~5 × 10^9 cfu/mL and stored in −80 °C. Each of the pools were subjected to deep sequencing of the insertion sites (Illumina HiSeq 2,500) to determine pool complexity, and the resulting information was submitted to NCBI Sequence Read Archive under accession No. PRJNA544499.

Tn-seq Screen: Growth of *L. pneumophila* Transposon Mutant Library in BMDM. Three of the transposon mutant library pools in *L. pneumophila* SK01 (*sde*$^+$) and SK02 (Δ*sde*) strains, encompassing 186,340 and 170,822 mutants based on deep-sequencing analysis, were independently diluted to A600 = 0.25 to 0.3, cultured to A600 = 0.3 to 0.4, diluted back to A600 = 0.2, and cultured in AYE to A600 = 3.8 to 4.0. Aliquots of each library pool grown in AYE were saved as input samples (T1) for growth in AYE broth, and then used to challenge BMDM at a multiplicity of infection (MOI) = 1 for 24 h. Cells were washed 3× at 2 h postinfection (hpi) with PBS, then replenished with fresh medium and further incubated for 24 h. BMDMs were then lysed in H_2O containing 0.05% saponin, and the diluted lysates were incubated on CYE plates with further incubation at 37 °C for 3 d. 1 to 7 × 10^6 colonies were harvested in AYE, mixed thoroughly, and used as the output sample (T2) for sequencing analysis. Genomic DNA from input and output samples was extracted using a QIAGEN DNeasy Blood and Tissue kit, including proteinase K prior to insertion-specific amplification and sequencing.

Transposon Sequencing and Fitness Calculation. Illumina™ sequencing libraries were prepared as described previously (44). Genomic DNA (40 ng) was tagmented in a 10 μL reaction mixture at 55 °C for 5 min, followed by inactivation at 95 °C for 30 s. Then, 40 μL of PCR mixture (First PCR), including primers 1st_TnR, Nextera2A-R and NEB Q5 high-fidelity polymerase (sequences of primers listed in *SI Appendix*, Table S1) was added to the tagmented samples to amplify transposon-adjacent DNA. The PCR amplification was performed by incubating at 98 °C for 10 s, 65 °C for 20 s and 72 °C for 1 min (30 cycles), followed by 72 °C for 2 min. After amplification, 0.5 μL of the PCR mixture was used in a second PCR reaction containing nested index primers (LEFT indexing primer specific for Mariner and RIGHT indexing primer) and Q5 polymerase in 50 μL total volume. The PCR conditions were 98 °C for 10 s, 65 °C for 20 s, and 72 °C for 1 min, followed by 72 °C for 2 min. Then, 9 μL of the PCR reaction was loaded and separated on a 1% agarose-Tris-acetate-EDTA (TAE) gel containing SYBR safe dye, and image intensity in the 250 to 600 bp region was quantified and pooled from each PCR product in equimolar amounts. The multiplexed libraries were purified on Qiagen QIAquick columns, with 17.5 pmol DNA then used in a 50 μL reconditioning reaction with primers P1 and P2 (*SI Appendix*, Table S1) and Q5 polymerase. The reaction was subjected to 95 °C for 1 min, 0.1 °C/s slow ramp to 64 °C for 20 s and 72 °C for 10 min. After PCR purification, multiplexed libraries were quantified, size-selected (250 to 600 bp; Pippin HT) and sequenced (single-end 50 bp) by Tufts University Genomics Core Facility. Sequencing was performed using Illumina HiSeq 2,500 with high-output V4 chemistry and custom primer with mar512.

Sequencing reads were processed (FASTX-toolkit), mapped to chromosome (AE017354) (Bowtie) and used to calculate individual transposon mutant fitness using a published pipeline (45). The fitness of an individual mutant (W_i) was calculated based on mutant vs population-wide expansion from T1 to T2 with following equation (46).

$$W\mathrm{i} = \frac{\ln(N_i(t_2)\hat{A}\hat{A}d/N_i(t_1))}{\ln((1-N_i(t_2))\hat{A}d/\hat{A}(1-N_i(t_1)))}$$

in which $N_i(t_1)$ and $N_i(t_2)$ are the mutant frequency at t_1 and t_2, respectively, and d is the population expansion factor. Transposon insertion sites located in the 5′- and 3′- terminal 10% of the open reading frame and genes having less than five insertions were excluded for further analysis.

Construction of *Legionella* Deletion Mutants. Individual genes were deleted in Lp02 strain by tandem double recombination using the suicide plasmid pSR47s as previously described (47). Primers used to construct all deletion plasmids are listed in *SI Appendix*, Table S1. Plasmids were propagated in *Escherichia coli* DH5α λpir.

Construction of Complementing Plasmids. To perform complementation experiments with genes encoded in trans on a replicating plasmid, pMMB207Δ267 (15, 48) was digested with *SacI-KpnI* and ligated with PCR-amplified DNA fragments encoding a 6xHis epitope tag, kanamycin resistance gene and *ccdB* flanked by *attR* recombination sites (gift of Tamara O'Connor), which was similarly digested, to generate a Gateway™-compatible destination

vector (pSK03; *SI Appendix*, Table S1). The individual genes were then cloned into the pSK03 plasmid by integrase cloning from a pDONR221-based IDTS plasmid library (49).

Intracellular Growth Assays. The intracellular replication of *L. pneumophila* was measured by luciferase activity using *ahpC::lux* derivatives of the WT and Δ*sde* strains (*SI Appendix*, Table S1). Bone marrow-derived macrophages (BMDM) were seeded in 96-well tissue culture plates at a density of 1×10^5 cells per well in RPMI medium without phenol read, containing 10% FBS (vol/vol) and 2 mM of glutamine. BMDMs were incubated at 37 °C containing 5% CO_2 and challenged with *L. pneumophila* Lux^+ strains at an MOI = 0.05, and luminescence was monitored every 30 min for 3 d during continuous incubation in an environmentally-controlled luminometer (Tecan).

Quantitative RT-PCR. PMA-differentiated U937 cells were seeded at a density of 4×10^6 cells per well in 6-well tissue culture plates. Cells were infected with postexponentially grown *L. pneumophila* Lp02 at an MOI = 20 and washed at 1 hpi. RNA was isolated using Trizol in accordance with the manufacturer's instructions. Contaminating genomic DNA was removed using the TURBO DNA-free kit, and cDNA was synthesized with 2.5 μg of RNA using the SuperScript VILO cDNA Synthesis Kit. PowerUp SYBR Green Master Mix was then used for qRT-PCR reactions using Second Step instrument (ABI). Transcriptional levels of genes were normalized to 16S rRNA. Oligonucleotides are listed in *SI Appendix*, Table S1.

Cytotoxicity Assays. 10^5 BMDMs were seeded per well in 96-well tissue culture plates and incubated overnight at 37 °C, 5% CO_2 prior to replenishing with 100 μL of medium containing propidium iodide (PI) at a final concentration = 20 μg/mL. Cells were challenged with 100 μL of postexponentially grown *L. pneumophila* Lp02 in the same medium at an MOI = 1 or 5 (36). Following infections, cells were centrifuged at 400× g for 5 min, incubated at 37 °C, 5% CO_2, and PI uptake was monitored every 10 min using the bottom reading setting in an environmentally controlled fluorometer (Tecan). To determine 100% cytotoxicity as the normalization control, cells were treated with 0.1% Triton X-100, and PI uptake was determined.

Assay for Vacuole Integrity. To measure the fraction of infected cells having intact *Legionella*-containing vacuoles (LCV), bacteria were centrifuged onto BMDMs for 5 min and incubated at 37 °C, 5% CO_2 for noted periods of time. The infection mixtures were then fixed in PBS containing 4% paraformaldehyde, then probed with mouse anti-*L. pneumophila* (Bio-Rad, Cat# 5625-0066, 1:10,000) followed by secondary probing with goat anti- mouse Alexa Fluor 594 (Invitrogen, Cat# A11005, 1:500), to identify permeable vacuoles as described (31). After washing 3× in PBS, LCVs were permeabilized by 5-min incubation with −20 °C methanol, prior to a second probing with mouse anti-*L. pneumophila*. All bacteria (both from intact and disrupted vacuoles) were identified by goat anti-mouse IgG Alexa Fluor 488 (Invitrogen, Cat# A11001, 1:500). The amount of vacuole disruption was quantified in two fashions. First, individual BMDMs were imaged using Zeiss observer Z1at 63× and scored for permeabilization based on staining with goat anti-mouse IgG-AlexaFluor 594 (antibody accessible in absence of methanol permeabilization) as described previously (32). To allow larger numbers of infected cells to be imaged, automated microscopy was performed using the Lionheart FX scanning microscope and Gen5 image prime 3.10 software. For detection of disrupted vacuoles (permeable in absence of methanol treatment), all images were analyzed by image preprocessing (10× magnification). To determine colocalization and quantification of vacuole integrity at 2 hpi, a primary mask was set for goat anti-mouse IgG-AlexaFluor 488 (detected after methanol treatment), and a secondary mask was set using a region that was expanded approximately 0.001 μm from the primary mask for goat anti-mouse IgG Alexa Fluor 594 (detected before methanol treatment). To identify intracellular bacteria, DAPI staining of nuclei was used to threshold a secondary mask 4 μm apart from the primary mask.

RTN4 Colocalization with LCV. RTN4 colocalization with the LCV was assayed by immunofluorescence microscopy. BMDMs were infected with *Legionella* strains for 4 h, fixed in PBS containing 4% paraformaldehyde, then extracted in 5% SDS to remove most of the cell-associated RTN4, then probed with mouse anti-*L. pneumophila* (Bio-Rad, Cat# 5625-0066, 1:10,000) and rabbit anti-RTN4 (Lifespan Biosciences, Cat# LS-B6516, 1:500) to detect detergent-resistant structures about the LCV. Bacteria were detected with anti-mouse Alexa fluor-594 and RTN4 structures with anti-rabbit Alexa Fluor-488 (Jackson ImmunoResearch, Cat# 711-545-152, 1:250). For quantification of total RTN4 intensity, we first set thresholds to determine ROIs (regions of interest) around the periphery of each bacterium in the Alexa 594 channel. These were then dilated by three pixels using the Yen routine in ImageJ, and the new preselected ROI from the Alexa 594 channel was applied to the Alexa 488 channel (green). Mean RTN4 intensity/pixel was measured in this dilated ROI and subtracted by background intensity/pixel obtained from uninfected cells in the same field of view using Fiji image analysis software (50).

Nucleofection. Differentiated BMDMs were seeded at a density of 5×10^6 cells in 10-cm dishes filled with 10 mL RPMI medium containing 10% FBS and 10% supernatant produced by 3T3- macrophage colony stimulating factor (mCSF) cells (51) and incubated overnight. Cells were lifted in cold PBS and resuspended in RPMI medium containing 10% FBS. Resuspended cells were aliquoted into 1.5-mL microfuge tubes containing 1×10^6 cells and pelleted at 200× *g* for 10 min. The pellets were resuspended in nucleofector buffer (Amaxa Mouse Macrophage Nucleofector Kit, Cat# VPA-1009) and 2 μg siRNA was added (siGENOME smart pool, Dharmacon). Cells were transferred to a cuvette and nucleofected in the Nucleofector 2b Device using Y-001 program settings according to the manufacturer's instructions. Nucleofected macrophages were immediately recovered in the medium and plated in eight-well chamber slides at 5×10^4 /well for microscopy assays or in 12-well plates at 1.5×10^5/well to prepare cell extracts for immunoblotting.

Immunoblotting. The efficiency of siRNA silencing in nucleofected cells was determined by immunoblot probing of SDS-PAGE fractionated proteins. Necleofected macrophages plated in 12-well plates were lysed by incubating in RIPA buffer (Thermo Fisher Scientific, Cat#89900) for 20 min on ice, and protein concentration was measured by BCA assay. In all, 5 to 10 μg of protein in SDS-PAGE sample buffer was boiled for 10 min, fractionated by SDS-PAGE and transferred to nitrocellulose membranes. The membrane was blocked in 50 mM Tris-buffered saline/0.05% Tween 20 (TBST, pH 8.0) containing 4% nonfat milk (blocking buffer) for 1 h at room temperature and probed with primary antibodies against Rab5B (Proteintech, Cat# 27403-1-AP, 1:1,000), SNX1 (Proteintech, Cat# 10304-1-AP, 1:1,000), RTN4 (Lifespan Biosciences, Cat# LS-B6516, 1:2,000), polyHistidine (Sigma-Aldrich, Cat# H1029, 1:2,000) and β-actin (Invitrogen, Cat# PA1-183, 1:1,000) in blocking buffer at 4 °C overnight. After washing 3× with TBST, the membranes were incubated with secondary antibody (Li-Cor Biosciences, Cat#926-32211, 1: 20,000) in blocking buffer for 45 min at room temperature. Capture and analysis were performed using Odyssey Scanner and the image Studio software (LI-COR Biosciences).

Assay for Bacterial Association with Host Cells. Bone marrow-derived macrophages (BMDM) were seeded in 96-well tissue culture plates at a density of 1×10^5 cells per well in RPMI medium containing 10% FBS (vol/vol) and 2 mM glutamine. BMDMs were then challenged with the indicated *L. pneumophila* strains at an MOI = 0.05 and incubated at 37 °C, 5% CO_2 atmosphere for indicated times. At either 10 min or 60 min postinfection, cells were washed 3× with PBS to remove extracellular bacteria, lysed with 0.05% saponin at 10 min or 60 min postinfection, and serial dilutions were potted on CYE plates to determine colony forming units [CFUs; (52).

Results

Identification of Genes Involved in LCV Biogenesis That Can Compensate for the Loss of Sde. We previously demonstrated that the *L. pneumophila* Δ*sde* strain (Δ*sidE* Δ*sdeABC*) is partially defective for growth within protozoan hosts, but grows in murine macrophages at levels close to that of the *L. pneumophila* WT strain (22, 53). This phenomenon is consistent with the existence of redundant Icm/Dot translocated substrates (IDTS) that can compensate for the lack of Sde proteins in mammalian hosts (15). To identify redundant pathways involved in intracellular growth, we performed transposon sequencing (Tn-seq) mutagenesis to uncover mutations that aggravate the Δ*sde* intracellular growth defect within bone marrow-derived macrophages (BMDMs). Transposon library pools were generated in both the WT and the Δ*sde* strain using the *Himar1* transposon, which specifically inserts at TA dinucleotides (54).

Three independently collected pools of *Himar-1* insertions were constructed in the *L. pneumophila* WT and Δ*sde* strains, encompassing 117,419 (47.33% of total TA sites) and 108,934 (43.91% of total TA sites) total unique insertions in the two genomes, respectively. This represented approximately 34 and 31 insertions/gene in WT and Δ*sde*, respectively (Dataset S1). After growth in broth to postexponential phase (T1) (55), BMDMs were challenged with both pools for 24 h (equivalent to a single round of infection; T2) and the fitness contribution of each mutation was determined during growth in broth and in BMDMs (Fig. 1*A* and *Materials and Methods*) (46). To identify genes that were required for intracellular replication in macrophages, the fitness difference between BMDM growth versus nutrient-rich medium growth was calculated in the WT and Δ*sde* strains, respectively (Fig. 1 *B* and *C*). Insertions in the majority of genes that were nonessential for growth in broth exhibited a fitness of ~1 during 24-h incubation in BMDMs, indicating that most genes are not required for intracellular growth in macrophages (*SI Appendix*, Fig. S1). It has been established that individual loss of only 6 IDTS (*mavN*, *sdhA*, *ravY*, Lpg2505, *legA3* and *lidA*) impair growth in macrophages, while individual loss of most of the other 300+ effectors show little defect in intracellular growth. This has been attributed to functional redundancy in *Legionella* secreted effectors (10, 30, 56–59). In our datasets, we confirmed those genes were required for replication in macrophages by WT (Fig. 1*B*, indicated by blue lettering). Furthermore, mutations in the preponderance of genes encoding translocator effectors generated no statistically significant defects in intracellular growth in either of the two backgrounds (Fig. 1 *B* and *C*), consistent with previous studies.

We then filtered mutations based on the following criteria: 1) causing lowered fitness relative to the population median, as defined by modified Z score > 1 (median absolute deviation (MAD) >1) and $P < 0.05$ based on unpaired t tests comparing mutations in the WT vs. Δ*sde* background (Dataset S1); 2) genes encoding *Icm/Dot* translocated substrates; and 3) genes encoding proteins thought to be involved in LCV biogenesis, based on published data. In addition, we identified mutations that showed no statistical defect in the WT, but whose fitness difference (Δ*sde* - WT) was > 1 MAD from the population median without any other consideration. Based on these criteria, three genes (*sdhA*, *ridL,* and *legA3*) were prioritized for further analysis (Fig. 1*D*; IDTS that passed criteria 1 and 2 are listed in Dataset S1, Gene Lists). SdhA protein is a T4SS substrate required for maintaining LCV integrity (30, 31). The absence of *sdhA* caused a growth defect in BMDMs infected with either WT or the Δ*sde* strains (Fig. 1 *B* and *C*). Even so, the fitness defect was significantly aggravated when *sdhA* was disrupted in the Δ*sde* strains relative to its loss in a WT strain background (Fig. 1*D*).

Mutations in *ridL* or *legA3* also showed aggravating growth defects in the Δ*sde* strains (Fig. 1*D*). RidL is a T4SS substrate that can inhibit function of the retromer complex that modulates retrograde traffic from early endosomes (40, 62). LegA3 is an ankyrin-repeat effector protein that is required for optimal replication in several hosts that has not been clearly tied to replication vacuole formation previously (15, 38, 43). Defective growth was specific to BMDMs as the double-mutant strains grew as well as the WT strain in bacteriological medium (Fig. 1*E* and Dataset S1). Most notably, based on their efficient growth in a WT

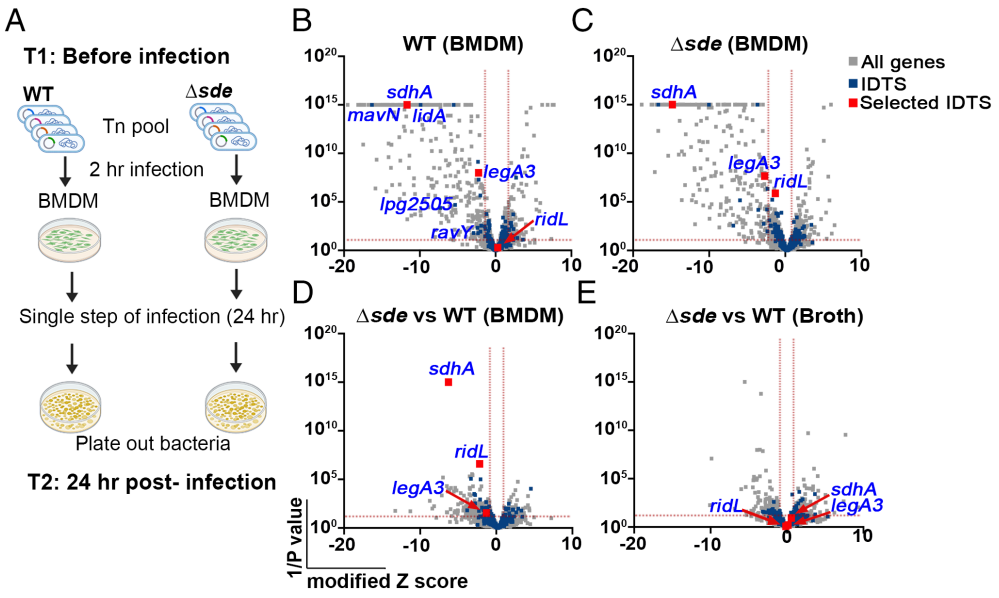

Fig. 1. Tn-seq identifies mutations that aggravate loss of Sde function. (*A*) Schematic view of Tn-seq analysis to identify aggravating mutations. *Himar-1* pools were constructed in parallel in SK01 (WT) and SK02 (Δ*sde*) strains, and insertion site abundance was determined after growth in broth (*Materials and Methods*). Three of the sequenced pools were incubated with BMDMs for 24 h in parallel, plated on bacteriological medium, and relative abundance of insertions was determined by HTS to determine fitness of individual mutations in the two different strain backgrounds (*Materials and Methods*). (*B* and *C*) Volcano plots of the relative fitness, represented as modified Z scores (*Materials and Methods*) comparing replication in BMDM versus AYE for either WT or Δ*sde* strains. Candidates were identified based on criteria of $Z_{MOD} > 2$ from the population median and were statistically significant ($P < 0.05$) based on unpaired *t* test after two-stage step-up correction (indicated by dotted red line) (60, 61). Blue font indicates IDTS that are the focus of study or which were previously shown to have an intracellular growth defect. (*D*) Volcano plots displaying relative fitness of insertion mutations in a Δ*sde* background compared to the WT background for intracellular growth in BMDM. Genes were identified as candidates based > 1 MAD from the population mean and statistical significance ($P < 0.05$) based on unpaired *t* test after two-stage step-up correction method (61) (indicated by dotted line). Data are based on n = 3 biological replicates of pools made in each strain. (*E*) Volcano plots of relative fitness (modified Z scores) of mutations in Δ*sde* background versus WT background for growth in AYE broth culture. Gray, blue, and red squares represent whole genes, *icm/dot* or Icm/Dot translocated substrate (IDTS) genes and genes selected based on the following criteria, respectively. Criteria: 1) mutations who showed fitness differences (Δ*sde* - WT) > 1 median absolute deviation (MAD) from the population median fitness and were statistically significant based on unpaired *t* tests ($P < 0.05$; Dataset S1), 2) genes that were *Icm/Dot* translocated substrates, and 3) genes possibly involved in LCV biogenesis.

background, was the behavior of insertions in *ridL*, which showed clear defects in a Δ*sde* background (Fig. 1 *C* and *D*)

The Absence of Sde Proteins Exacerbates Intracellular Growth Defects of *sdhA*, *ridL*, or *legA3* Deletion Mutants. To verify that the phenotypes predicted by the parallel Tn-seq pools can be reproduced at the single-strain level, in-frame deletion mutations in *sdhA, ridL, and legA3* were generated in both the WT and Δ*sde* strain backgrounds harboring the luciferase (*ahpC*::*lux*$^{+}$) reporter. The respective mutations were confirmed by whole-genome sequencing (PRJNA864753), and intracellular growth of *L. pneumophila* strains was then monitored by luminescence accumulation after incubation with BMDMs. As predicted by the Tn-seq analysis, combining the loss of Sde proteins with the Δ*ridL* mutation revealed a growth defect that did not exist in the absence of the combination. In the presence of the Sde proteins, the Δ*ridL* strain showed no growth defect after challenge of BMDMs. In contrast, introduction of Δ*ridL* into the Δ*sde* strain resulted in yields that were 100× lower relative to the WT and approximately 10× lower relative to the parental Δ*sde* strain after 72-h incubation (Fig. 2*A*). Additionally, catastrophic synergistic defects were observed with the Δ*legA3* mutation after introduction into the Δ*sde* background. In an otherwise WT background, loss of either Sde proteins or RidL resulted in mild growth defects after 72-h incubation. The Δ*sde*Δ*legA3* strain, however, showed little or no evidence of growth during this time period (Fig. 2*B*). Finally, although the Δ*sdhA* strain reproduced the previously documented growth defect in BMDMs (30, 31), combination with Δ*sde* resulted in a strain that showed yields similar to the type IV secretion system defective *dotA*$^{-}$ strain (Fig. 2*C*)

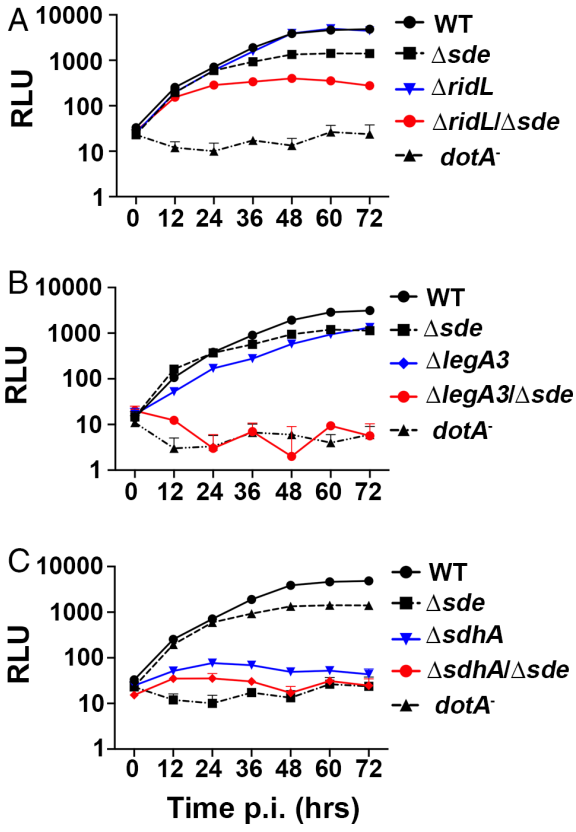

Fig. 2. Identification of mutations that aggravate the intracellular growth defect of Δ*sde*. (*A–C*) BMDMs were challenged with WT (Lp02) or noted *L. pneumophila* mutants expressing luciferase (P*ahpC*::lux). Intracellular growth was determined by measuring luminescence hourly. Data shown and error bars are mean ± SEM at 12 h increments (mean of three technical replicates and a representative of three biological replicates).

Aggravation of the Δ*sde* Lesion Causes Premature Host Cell Death Due to Destabilization of the LCV. To determine if there were a clear defect in replication vacuole biogenesis associated with aggravating the loss of Sde function, we took advantage of the fact that SdhA is required to maintain integrity of the LCV, reasoning that the absence of Sde could exacerbate this defect (31, 32). As had been noted previously, challenge with a Δ*sdhA* strain resulted in a significant fraction of the LCVs becoming permeable and accessible to antibody penetration at 6 h postinfection (hpi) (*SI Appendix*, Fig. S2) (31). At 2 hpi, however, there is no evidence that the absence of SdhA interferes with LCV integrity, with both the WT and Δ*sdhA* strains showing indistinguishable levels of permeability to antibody staining (*SI Appendix*, Fig. S2). As Sde proteins act to remodel Rtn4 about the replication vacuole within 10 min of bacterial challenge (22, 53), we reasoned that any compensation for loss of SdhA should occur at early timepoints. To determine a specific timepoint, we measured the relative transcription of each individual gene after bacterial contact of a WT strain with cultured cells. The expression of *sdeA* and *sdeC* dropped only slightly from 1 to 2 hpi, but dramatically decreased by about 10-fold at 6 hpi compared to that at 1 hpi (*SI Appendix*, Fig. S3). Therefore, we sought to examine the integrity of the LCV in BMDMs at 2 hpi when the contribution of the Sde family should be the highest.

Vacuole integrity of the mutants was evaluated by probing fixed BMDM with anti-*L. pneumophila* in the presence or absence of chemical permeabilization, using our previously established immunofluorescence staining method (Fig. 3*A*) (31). Surprisingly, even the Δ*sde* single mutant strain generated a higher frequency of permeable vacuoles than WT at the 2-h timepoint (Fig. 3*B*). In contrast, *ridL*, *legA3,* and even *sdhA* single deletions showed vacuole permeability frequencies that were comparable to WT at this timepoint (Fig. 3*B*). The most dramatic effects were observed when deletions of *sdhA*, *ridL*, and *legA3* were introduced into the Δ*sde* strain. Addition of each individual deletion to the Δ*sde* mutant severely aggravated the vacuole integrity defect, resulting in up to fourfold more permeable vacuoles, indicating that these mutation combinations drastically destabilized the LCV (Fig. 3*B*).

To allow larger numbers of LCVs to be analyzed (1,000 to 3,000 per biological replicate), albeit at lower resolution, we used a lower power objective to repeat the analysis. Although low-power analysis made it more difficult to identify permeable vacuoles, the results were in concordance with those displayed in Fig. 3*B* (*SI Appendix*, Fig. S4). These results indicate that at early timepoints after infection, the *L. pneumophila* has redundant T4SS substrates that can compensate for the loss of Sde, and that vacuole disruption resulting from absence of *sde* is potentiated by the addition of secondary mutations in *sdhA*, *ridL,* and *legA3*. To exclude the possibility that the differences we observed in LCV disruption are driven by the double mutants having faster uptake kinetics, which could elicit a faster host response (63), association with BMDMs was compared and shown to be indistinguishable among all strains at 10 or 60 min postinfection (*SI Appendix*, Fig. S5).

Pyroptotic cell death occurs as a consequence of a comprised LCV membrane followed by bacterial exposure to the macrophage cytosol (31). Based on the loss of LCV barrier function shortly after initiation of infection, we hypothesized that the respective Δ*sdhA*Δ*sde*, Δ*legA3*Δ*sde* and Δ*ridL*Δ*sde* double-mutant strains should accelerate BMDM cell death in comparison to either the WT or single mutants. To this end, cytotoxicity assays were

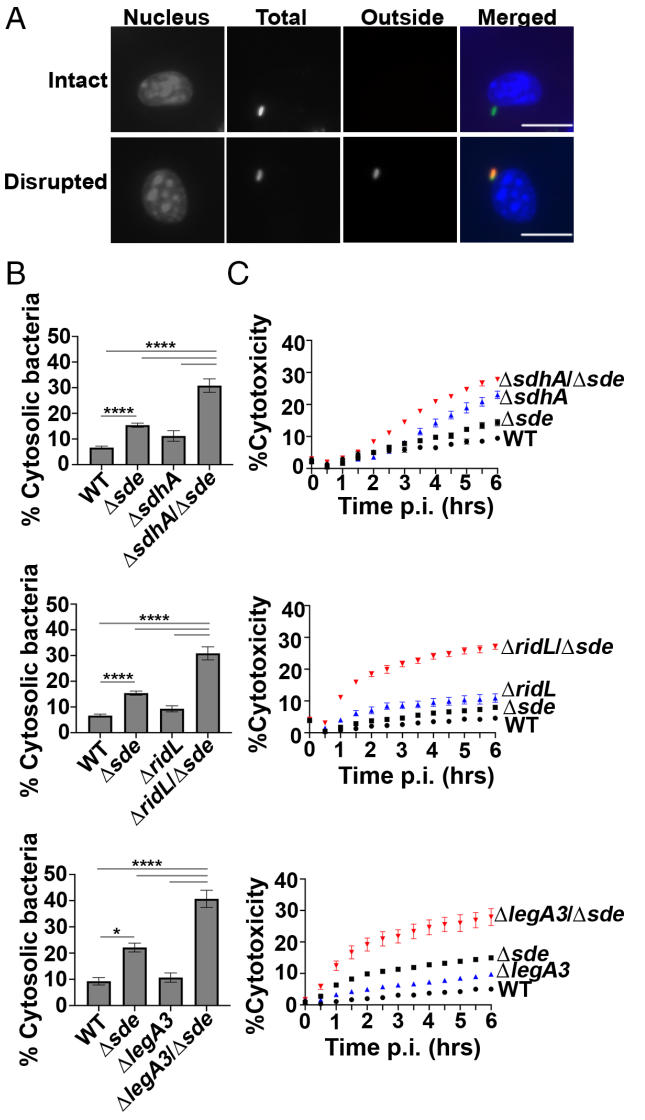

Fig. 3. Aggravating mutations result in loss of LCV integrity and accelerated pyroptotic cell death at early infection times. (*A*) Examples of cytosolic and vacuolar bacteria. Macrophages were challenged with either WT or noted mutant strains for 2 h, fixed, probed with anti-*L. pneumophila* (Alexa Fluor 594 secondary, red), permeabilized, and reprobed with anti-*L. pneumophila* (Alexa Fluor 488 secondary, green). Cytosolic bacteria are accessible to both antibodies, shown in yellow in the merged image, whereas vacuolar bacteria are shown in green. The scale bar represents 10 μm. (*B*) Disrupted vacuole integrity of *L. pneumophila* strains at 2 h post-infection. BMDMs were challenged with indicated strains, fixed, and stained for bacteria before and after permeabilization. For quantification, bacteria that stained positively in the absence of permeabilization were divided by the total infected population (mean ± SEM; three biological replicates with 300 LCVs were counted per replicate) (*C*) Kinetics of macrophage cell death, with infection of indicated strains. BMDMs were infected with *L. pneumophila* WT or mutant strains and propidium iodide (PI) incorporation was used to monitor cell death. Data shown and error bars are mean ± SEM for 30 min increments and a representative of three biological replicates. Statistical analysis was performed using one-way ANOVA with Tukey's multiple comparisons, with significance represented as: *$P < 0.05$; ****$P < 0.0001$.

performed, assaying for propidium iodide (PI) access to the macrophage nucleus [*Materials and Methods* and (36). In perfect concordance with the loss of LCV integrity, pyroptotic cell death was exacerbated when mutations in either *sdhA*, *ridL,* and *legA3* were combined with Δ*sde* (Fig. 3*C*). Accessibility to PI was more rapid than that observed with the WT, and the total cytotoxicity plateaued at levels that far exceeded the WT during the course of the experiment, consistent with the early defect of these double mutants resulting in increased overall damage to the LCV relative to the WT.

pR-Linked Ubiquitinated RTN4 Is Required for LCV Integrity. To demonstrate that expression of single Sde effectors was sufficient to restore LCV integrity in the absence of SdhA function, plasmids encoding individual effectors were introduced into the Δ*sde*Δ*sdhA* strain. As expected, the introduction of plasmid-encoded *sdhA* resulted in increased LCV integrity relative to the double mutant, as measured by the antibody accessibility assay (Fig. 4*A*). Similarly, plasmids encoding single Sde effectors (*sdeA*, *sdeB*, *sdeC*: Fig. 4*A*) introduced into the Δ*sde*Δ*sdhA* strain that approached levels of LCV protection observed with the Δ*sdhA* strain ($P = 0.5$ to 0.98, one-way ANOVA, Tukey's multiple comparisons). To probe if pR-Ub linked RTN4 is required for stabilizing vacuole integrity, plasmids expressing $SdeB_{WT}$ or its catalytic mutant derivatives (C118S, inactive DUB; H416A, inactive NP, E859A, inactive mART) were introduced into the Δ*sde*Δ*sdhA* strain. The plasmid harboring $SdeB_{H416A}$ (defective in generating/transferring pR-Ub to RTN4) or $SdeB_{E859A}$ (defective in ADP-ribosylation of Ub) could not protect from vacuole disruption in the Δ*sde*Δ*sdhA* strain (Fig. 4*B*; compare vector vs H416A or E859A), whereas $SdeB_{C118S}$ showed a comparable level of complementation to the strain harboring the $SdeB_{WT}$ plasmid (Fig. 4*B*). The complementation data were consistent with the levels of Rtn4 associated with the replication vacuole for each of these derivatives, as mutants that failed to complement also failed to show Rtn4 association, as observed previously [Fig. 4*C* and (22). We conclude that phosphoribosyl-linked ubiquitination of Rtn4 and its associated Rtn4 rearrangements are required to allow protection of the LCV from degradation in the absence of SdhA function.

Downmodulation of Sde Activity by SidJ Interferes with Vacuole Protection. Sde proteins were only able to compensate for loss of SdhA at early times after infection of BMDMs, as accumulation of degraded LCVs was observed in a Δ*sdhAsde*$_{WT}$ strain at later times postinfection [*SI Appendix*, Fig. S2 and (31). An explanation for this phenomenon is that protection of the LCV by Sde proteins is negatively regulated in a temporal fashion by the SidJ meta-effector, which shuts down Sde activity by glutamylation of the active site on Sde mART domain (28). The primary consequence of this posttranslational modification is that Sde proteins are released from the LCV (26). In addition, SidJ shutdown of phosphoribosyl-linked ubiquitination should prevent the accumulation of proteins such as Rtn4 about the LCVs. Therefore, the absence of SidJ is predicted to prolong Sde activity and consequently compensate for loss of SdhA as the infection proceeds. To test this hypothesis, a deletion of *sidJ* was introduced into the Δ*sdhA* strain, and vacuole integrity was examined at 4 hpi (Fig. 5*A*). Based on the antibody protection assay, there was ~33% reduction in degraded vacuoles resulting from the absence of SidJ from the Δ*sdhA* strain. This result is consistent with Sde activity reversing loss of SdhA at 4 hpi (Fig. 5*A*; compare Δ*sidJ*Δ*sdhA* to Δ*sdhA*).

Deletion of SidJ did not completely protect from vacuole disruption, as infection with the Δ*sdhA*Δ*sidJ* only partially phenocopied a WT strain, indicating that pR-Ub-linked targets likely persist for extended periods of time in the presence of intact SidJ function (WT compared to Δ*sidJ*Δ*sdhA*; Fig. 5*A*). One likely candidate for persistent modification is RTN4 (Fig. 5*B*), which forms detergent-resistant aggregates that may slowly dissipate in the absence of continued modification by Sde proteins. To determine if vacuole disruption is connected to partial loss of RTN4 aggregates, the intensity of Rtn4

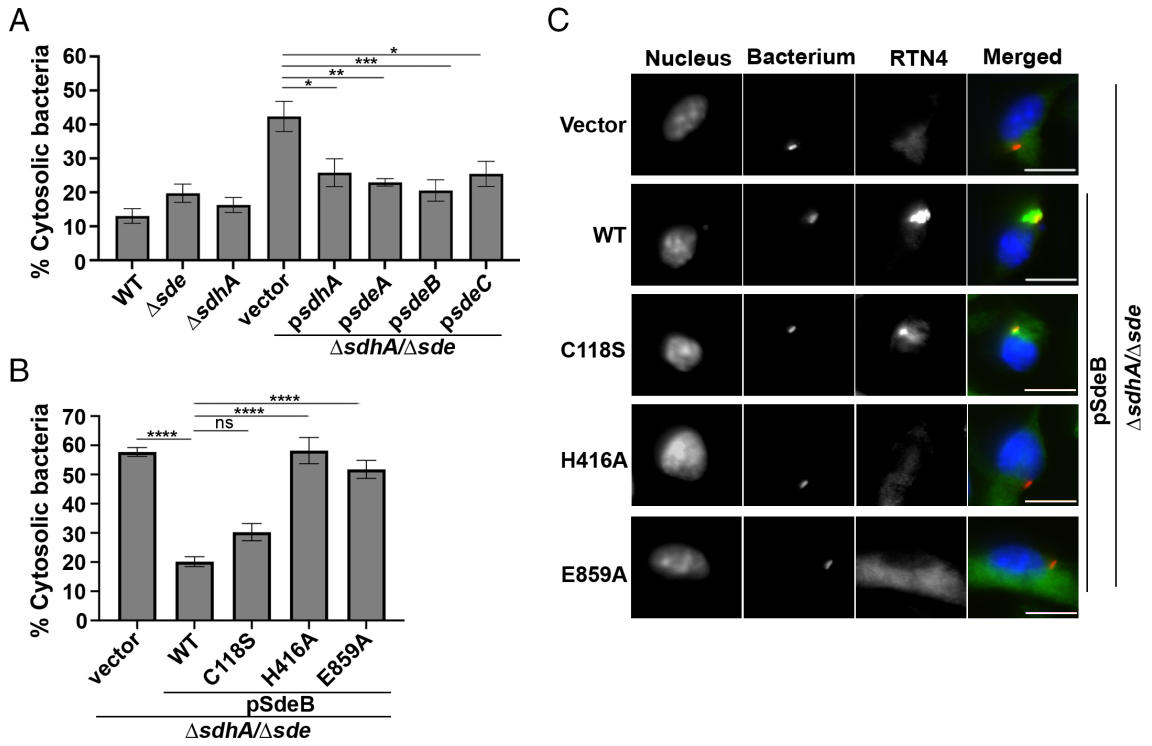

Fig. 4. Sde-mediated pR-modified RTN4 is required for protection of LCV integrity. (*A* and *B*) Vacuole integrity of *L. pneumophila* strains at 2 h postinfection. BMDMs were challenged with indicated strains that harbor either empty vector or vector expressing noted genes, fixed and stained for bacteria before and after permeabilization. The percentages of cytosolic bacteria were calculated (*Materials and Methods*). Data displayed are mean ± SEM for three biological replicates. Statistical significance was tested using one-way ANOVA with Tukey's multiple comparisons; ns (non-significant), $^{*}P < 0.05$, $^{**}P < 0.01$, $^{***}P < 0.001$, $^{****}P < 0.0001$. (*C*) Complementation of Δ*sdh*AΔ*sde* strains requires pR-Ub modification of target. Shown are images of BMDMs challenged with *L. pneumophila* Δ*sdh*AΔ*sde* harboring plasmid-encoded *sdeB* or its derivatives (C118S, inactive DUB domain; H416A, inactive NP domain; E859A, inactive mART domain) and probed for detergent-resistant association of RTN4 after fixation (*Materials and Methods*). (Scale bar, 10 μm.)

aggregates around the LCV was quantified microscopically after detergent extraction (Fig. 5*C* and *Materials and Methods*). Consistent with expectations, the total amount of RTN4 associated with the LCV was increased by removing SidJ (Fig. 5*C*). This effect was independent of the presence of the *sdhA*, as the absence of SidJ in both WT (Fig. 5*C*; WT vs Δ*sidJ*) and Δ*sdhA* strains (Fig. 5*C*; Δ*sdhA* vs. Δ*sidJ*Δ*sdhA*) resulted in higher levels of Rtn4 accumulation at 4 hpi. Therefore, loss of SidJ lengthens the time that Sde function can compensate for the absence of SdhA and is associated with increased accumulation of Rtn4 at this timepoint. Parenthetically, it should be noted that a Δ*sdhA* strain showed lower levels of Rtn4 accumulation than that observed with WT (although not statistically significant in this assay). Presumably, as vacuoles degrade in the Δ*sdhA*, fragments are shed from the LCV harboring either Sde proteins or Rtn4, resulting in lowered Rtn4 accumulation.

LCVs Harboring Strains Lacking *Sde* Are Stabilized by Depletion of Proteins Involved in Early Endocytic and Retrograde Trafficking. Based on work from both *Salmonella* and *Legionella*, the most common explanation for bacterial mutants that result in destabilization of the pathogen replication vacuole is that there is a failure to protect from association with host membrane compartments that result in vacuole degradation (37, 64). For example, SdhA antagonizes function of the early endocytic compartment, in part by diverting the OCRL phosphatase (32, 37). As a consequence, depletion of components that regulate early endocytic dynamics, such as Rab5bB, prevents LCV degradation, stabilizing the replication niche in the absence of SdhA (32, 37, 65, 66). To determine if Sde and SdhA proteins protect the LCV from attack by the same host membrane trafficking pathways, depletion with small interfering RNA (siRNA) against Rab5B in BMDMs was performed and vacuole integrity was measured at 2 hpi. At this timepoint, when Sde proteins appear to be the primary stabilizers of the LCV, knockdown of Rab5B partially reversed vacuole disruption after challenge with the Δ*sdhA*Δ*sde* strain (Fig. 6*A*). This indicates that Sde and SdhA are likely able to interfere with the same early endocytic pathway. As expected, no restoration was observed in cells infected with WT, although the corresponding single Δ*sde* strain, which shows a small defect in maintaining vacuole integrity, was unaffected by the loss of Rab5B (Fig. 6*A*). Therefore, in the absence of Rab5B, there may be another pathway that Sde proteins directly antagonize to promote vacuole integrity.

We previously demonstrated that knockdown of Rab11, a GTPase that regulates the recycling endosome, partially rescues the vacuole integrity defect of a Δ*sdhA* strain. This indicates that host recycling compartments interfere with vacuole integrity (37). Furthermore, Sorting Nexin 1 (SNX1) participates in these events, drives Rab11 recycling and functions in tandem with the Retromer, which is a target of RidL (39, 40, 67, 68). We thus predicted that the depletion of SNX1 should also reverse vacuole disruption. To this end, SNX1 was depleted by siRNA prior to bacterial infection and vacuole integrity was measured at 2 hpi. In this case, the ability to partially rescue the vacuole integrity defect at an early timepoint was independent of *sdhA* function. For both the Δ*sde* and Δ*sde*Δ*sdhA* strain backgrounds, depletion of SNX1 resulted in a significant reduction of disrupted vacuoles, with 50% and 38% fewer antibody-permeable vacuoles observed in the presence of siRNA directed toward SNX, respectively, when compared to

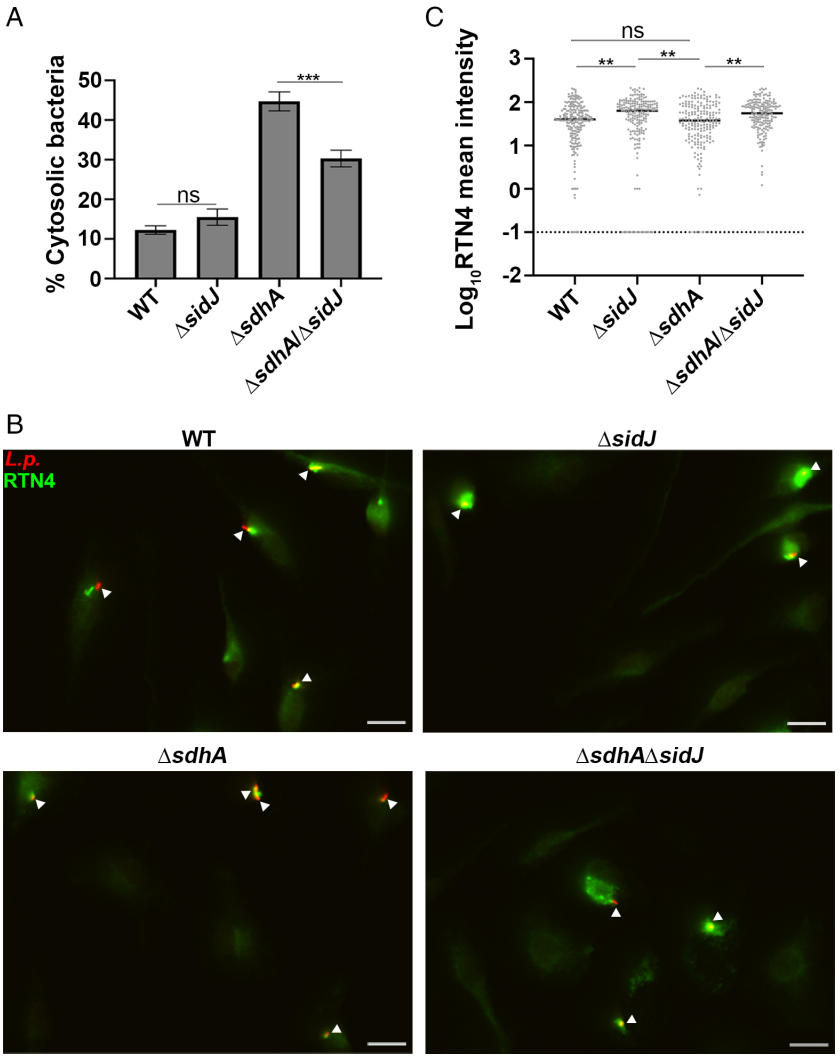

Fig. 5. Increased aggregation of RTN4 is associated with maintenance of LCV integrity. (*A*) Vacuole integrity of *L. pneumophila* strains at 4 h postinfection. At least 70 LCVs were counted per replicate and data shown as mean ± SEM for four biological replicates. (*B*) Representative micrographs of RTN4 associated with individual LCVs after detergent extraction of fixed samples, (Scale bar, 10 μm.) (*C*) Loss of SidJ results in increased association of RTN4 about LCV. Images of individual LCVs were captured and pixel intensities of RTN4 staining about regions of interest were determined (*Materials and Methods*). Displayed are mean pixel intensities about the LCV associated with each mutant (*Y* axis). The dotted line shows the LCVs that have background RTN4 intensity. More than 60 LCVs were quantified per experiment, and data were pooled from three biological replicates. Statistical significance was tested using one-way ANOVA with Tukey's multiple comparisons (*A*) or Kruskal–Wallis test (*C*); ns (non-significant), $^{**}P < 0.01$, $^{***}P < 0.001$.

treatment with the scrambled control (Fig. 6*B*). These results support previous work that early endosome dynamics are involved in disrupting the LCV and are consistent with Sde proteins playing a special role in blocking SNX1/retromer-mediated membrane traffic at early timepoints after bacterial challenge of primary macrophages.

Discussion

Replication vacuole integrity is a critical determinant of successful pathogen growth within membrane-bound compartments (69). The importance of this process has been demonstrated for several intracellular pathogens, all of which encode proteins critical for maintaining an intact vacuolar barrier (31, 70–72). In each case, bacterial proteins appear to interfere with the function of membranes exiting from early endosomal/recycling compartments (32, 37, 40). There is no clear explanation for how endosomal membranes disrupt replication compartments, but bacterial mutant studies indicate that the replication vacuole has a unique membrane composition that is destabilized by endosomal membranes (73). In particular, *S. typhimurium* and *L. pneumophila* mutants lacking specific phospholipases stabilize these compartments (31, 74). In the case of *L. pneumophila plaA* mutations, loss of a lysophospholipase reduces the fraction of permeable LCVs observed in *sdhA* mutants, indicating that modulation of lysophospholipid content may maintain replication vacuole integrity. In fact, analysis of the *L. pneumophila* translocated effector VpdC argues that lysophospholipid content regulates LCV expansion, consistent with vacuole integrity being dependent on homeostatic control of lysophospholipids (75).

In this report, we obtained the surprising result that the *L. pneumophila* Sde proteins contribute to maintaining LCV integrity (Fig. 3). The fact that depletion of factors involved in endosomal trafficking resulted in partial rescue of the Δ*sde* mutant is consistent with components of the endosomal pathway destabilizing the LCV in the absence of Sde function. (Fig. 6). Loss of SdhA or RidL aggravated the minor growth defect of a Δ*sde* strain, thereby eliminating proteins that interface directly with endosomal factors (Fig. 1). In the case of SdhA, the protein engages and diverts the OCRL phosphatase endosomal traffic regulator, while RidL prevents activation of retromer components that modulate retrograde traffic from endosomes (32, 40, 41, 62). Sde proteins may work in a very different fashion than these two proteins. Sde proteins catalyze phosphoribosyl-linked modification of a large number of host proteins, modifying Ser and perhaps Tyr residues on protein targets (19, 76). An early target is the endoplasmic reticulum protein Rtn4, which is not known to directly interface with the endosomal system (22). Large-scale identifications of proteins modified by SdeA confirm that Rtn4 is among the most abundant pR-UB-linked proteins (24, 25).

The connection between Rtn4-mediated ER rearrangements and support of membrane integrity raises the possibility that

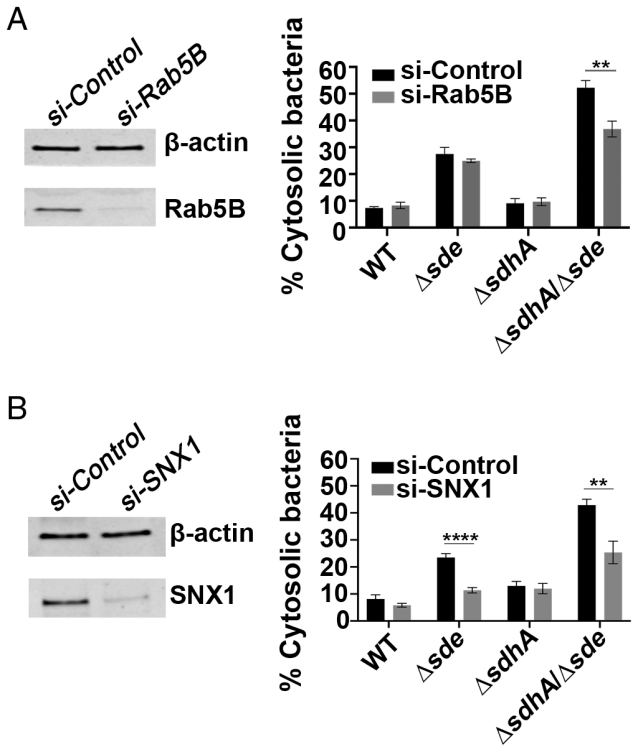

Fig. 6. Interference with host endocytic and retromer-mediated trafficking pathways allows partial rescue of vacuole integrity defect. (*A*) Effect of si-Rab5B on vacuole integrity. (*A*, *Left*) immunoblot of SDS-polyacrylamide gel probed with anti-Rab5B after depletion with si-Rab5B or control scrambled si-RNA. (*A*, *Right*) the percentage of cytosolic bacteria from BMDMs treated with si-Control or si-Rab5B, and challenged with noted *L. pneumophila* strains for 2 h, followed by probing as described (*Materials and Methods*). (*B*) Effect of si-SNX1 on vacuole integrity. (*B*, *Left*) immunoblot of SDS-polyacrylamide gel probed with anti-SNX1 after depletion with si-SNX1 or control scrambled si-RNA. (*B*, *Right*) the percentage of cytosolic bacteria from BMDMs treated with si-Control or si-SNX1 and challenged with noted *L. pneumophila* strains for 2 h, followed by probing as described (*Materials and Methods*). For immunoblotting, β-actin was used as loading control. The data shown are mean ± SEM, using three biological replicates, with at least 100 LCVs counted per biological replicate. Statistical analysis was conducted using unpaired two-tailed Student's *t* test and significance displayed as $^{**}P < 0.01$ or $^{****}P < 0.0001$.

Sde action protects the LCV from host attack by forming a shield about the LCV. To interrogate the role of RTN4 in stabilizing LCV integrity, we have tested if mutational loss of Rtn4 could phenocopy the Δ*sde* mutation at 2 hpi. Infection of *rtn4*$^{-/-}$ macrophages with *L. pneumophila* Δ*sdhA* generated an increased fraction of permeable vacuoles compared to infection of *rtn4*$^{+/+}$ BMDMs. This result strongly supports a role for Rtn4 in stabilizing LCV integrity as a consequence of Sde activity (77).

Immediately after *L. pneumophila* contact with mammalian cells, Sde proteins drive abundant accumulation of Rtn4-rich tubular ER aggregates (Fig. 7). These structures result in complex pseudovesicular structures, observed over 20 y ago in both mammalian cells and amoebae within 10 min postinfection (14, 22, 78). Over time, these structures dissipate and are replaced by rough ER (14, 78). Therefore, regulation of Sde function ensures that it operates primarily during the initial stages of replication. This explains why loss of SdhA has little effect on LCV integrity during the first 2 hpi (Fig. 3), and only shows a defect when combined with loss of Sde function. Consequently, SdhA primarily plays a backup role during the first 2 hpi (Fig. 7), but when Rtn4-rich pseudovesicular structures dissipate at later time points (22, 53), SdhA assumes its role as the primary essential guard against LCV disruption.

Based on these results, we propose a model in which Sde, RidL, and SdhA promote LCV integrity in a temporally controlled fashion (Fig. 7). Shortly after infection, we hypothesize that the Sde proteins act to wall off the LCV from endosomal attack by rearranging tubular ER into dense structures as a consequence of pR-UB-modification of Rtn4 (22). RidL and SdhA are present on the LCV to protect against occasional breaches of this barrier at early time points (32, 40). The continued presence of the physical barrier, however, is likely to pose problems for supporting bacterial growth because it prevents access of the LCV to either metabolites or lipid biosynthesis components. This predicts that optimal growth of *L. pneumophila* must involve the breakdown of the pR-Ub-modified physical barrier. Therefore, metaeffectors that reverse Sde family function, such as the SidJ protein (27–29), are necessary for optimal intracellular growth because they facilitate barrier breakdown (26, 79). Consistent with this model, there is suboptimal growth in the absence of SidJ (26, 79), with the negative consequence that *L. pneumophila sidJ*$^{-}$ mutants accumulate Rtn4 at the 4 h timepoint (Fig. 5). To avoid a tradeoff between supporting vacuole integrity and interfering with intracellular growth, *L. pneumophila* has acquired the ability to disrupt the Sde-promoted barrier, necessitating the localization of the SdhA vacuole guard on the LCV to protect a point of vulnerability for the replication niche (Fig. 7).

This work provides a fresh view of the role of redundancy in an intracellular pathogen. In the case of protecting LCV integrity, our work argues that multiple proteins do not work in parallel pathways toward the same end. Instead, each pathway is temporally controlled, playing an important role at different times in the replication process. This then explains the profound replication defect of a *sdhA*$^{-}$ strain, which only has some low-level support from RidL and residual remnants of the Sde-targeted protein blockade. The lack of effective backup pathways as the replication cycle proceeds necessitates the upregulation of SdhA, resulting in a largely nonredundant role for this protein (*SI Appendix*, Fig. S3). That RidL and LegA3 are not particularly effective backups for SdhA as the infection cycle proceeds, indicates that these proteins may be unable to block critical membrane-disruptive pathways that are inactivated by SdhA.

An important caveat to this model is that Sde protein can target a number of proteins other than Rtn4 (16, 24, 25). Furthermore, Sde localization is not restricted to the LCV, but family members can be found on a number of organelles, including endosomes/lysosomes and mitochondria at early stages of infection (~ 1 h postinfection) (26). In this regard, we think it likely that there are two modes of action that can promote vacuole integrity. One mode is to establish a physical barrier around the LCV by eliciting Rtn4-ER rearrangements. The other is to modify host proteins associated with endocytic trafficking, Golgi biogenesis, or autophagy (24). In this regard, partial rescue of the LCV integrity defect by depletion of SNX1 in BMDMs infected with Δ*sde* mutants is particularly noteworthy (Fig. 6*B*). Previous studies have shown that SNX1 is localized on LCVs, raising the possibility that proteins controlling the movement, docking and fusion of disruptive compartments could come in contact with Sde proteins and allow inactivation of these compartments (24, 40). Therefore, Sde proteins may act as their own backup factors, inactivating disruptive compartments that sneak through the Rtn4-aggregated barrier.

In summary, by performing parallel dense transposon mutagenesis in matched strains, we have obtained evidence that the Sde family acts to protect the LCV from disruption by the host. Furthermore, our study provides a framework for vacuole guard

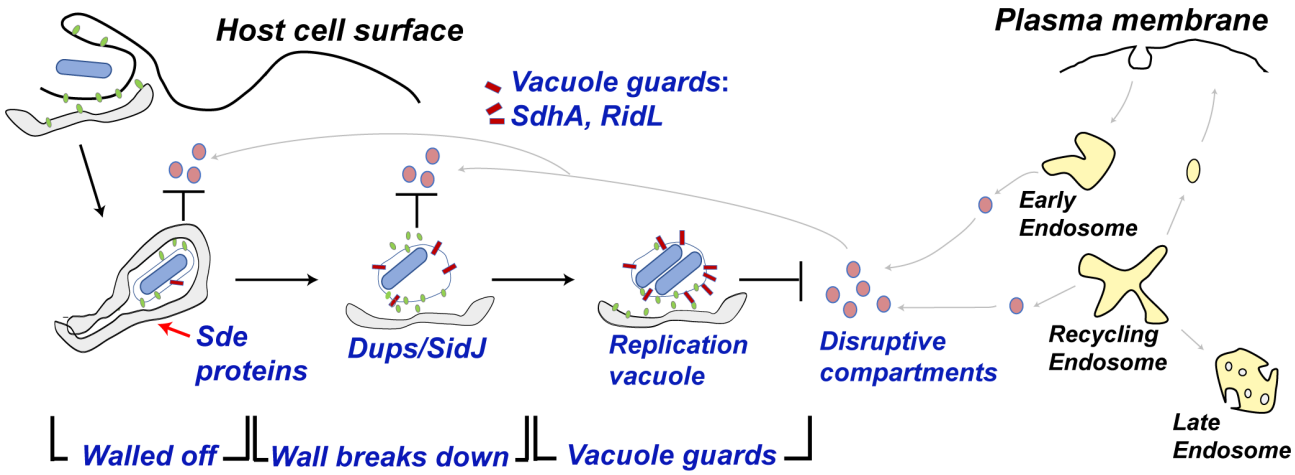

Fig. 7. Schematic model of how *Legionella* combats vacuole disruption in a temporally-regulated process. Soon after internalization, the *Legionella* containing vacuole is walled off with RTN4-rich tubular ER aggregates as a consequence of pR-Ub modification of RTN4 by Sde proteins (22). Step 1. Walled off: at early time of infection, the barrier as well as SdhA and RidL (backup vacuole guards in case the barrier is breached) protects the LCV from host membrane traffic derived from the early/recycling endosome. Step 2. Wall Breaks Down: over time, the wall is breached as the aggregates are dissipated by SidJ, a metaeffector that inactivates Sde proteins, (26–29) and Dups (DupA and DupB), enzymes that deubiquitinate pR-Ub-linked substrates (24). Step 3. Vacuole guards: when the barrier around the LCV is dismantled, SdhA and RidL act to divert and inactivate disruptive compartments derived from the early/recycling endosomes to allow the LCV to be replication-permissive (25, 32, 37).

function, as the described guards are temporally regulated to maximize the replication potential of *L. pneumophila*. Future work will focus on how manipulation of host membrane compartments leads to maintaining LCV integrity, and determining the molecular details for how LCV disruption occurs in the absence of vacuole guards.

Data, Materials, and Software Availability. Scripts used for sequencing read analysis can be found at http://github.com/vanOpijnenLab/MaGenTA. All sequence data are deposited in the NCBI Sequence Read Archive under accession numbers: PRJNA544499, PRJNA847256 and PRJNA864753 (WGS data). All study data are included in the article and/or supporting information.

ACKNOWLEDGMENTS. We thank Dr. Joseph Vogel for the kind gift of the *Legionella* strain (Δ*sidJ*), Drs. Ila Anand and Mengyun Zhang for preliminary work indicating that SNX1 contributes to driving LCV disruption, and Dr. Philipp Aurass for discussions regarding analysis of Tn-seq results. We thank Juan Hernandez-Bird, Mitchell Berg, and Drs. Wenwen Huo, Philipp Aurass and Kevin Manera for review of the text. This work was supported by NIAID Awards 5R01-AI46245 and 5R01-AI113211 to (R.R.I.).

1. T. J. Rowbotham, Preliminary report on the pathogenicity of *Legionella pneumophila* for freshwater and soil amoebae. *J. Clin. Pathol.* **33**, 1179–1183 (1980).
2. T. W. Nash, D. M. Libby, M. A. Horwitz, Interaction between the legionnaires' disease bacterium (*Legionella pneumophila*) and human alveolar macrophages. Influence of antibody, lymphokines, and hydrocortisone. *J. Clin. Invest.* **74**, 771–782 (1984).
3. T. M. Nguyen *et al.*, A community-wide outbreak of legionnaires disease linked to industrial cooling towers–how far can contaminated aerosols spread?. *J. Infect Dis.* **193**, 102–111 (2006).
4. M. A. Horwitz, S. C. Silverstein, Legionnaires' disease bacterium (*Legionella pneumophila*) multiples intracellularly in human monocytes. *J. Clin. Invest.* **66**, 441–450 (1980).
5. W. Zhu *et al.*, Comprehensive identification of protein substrates of the Dot/Icm type IV transporter of *Legionella pneumophila*. *PLoS One* **6**, e17638 (2011).
6. Z. Q. Luo, R. R. Isberg, Multiple substrates of the *Legionella pneumophila* Dot/Icm system identified by interbacterial protein transfer. *Proc. Natl. Acad. Sci. U.S.A.* **101**, 841–846 (2004).
7. L. Huang *et al.*, The E Block motif is associated with *Legionella pneumophila* translocated substrates. *Cell Microbiol.* **13**, 227–245 (2011).
8. Z. Lifshitz *et al.*, Computational modeling and experimental validation of the *Legionella* and *Coxiella* virulence-related type-IVB secretion signal. *Proc. Natl. Acad. Sci. U.S.A.* **110**, E707–715 (2013).
9. L. Gomez-Valero *et al.*, More than 18,000 effectors in the *Legionella* genus genome provide multiple, independent combinations for replication in human cells. *Proc. Natl. Acad. Sci. U.S.A.* **116**, 2265–2273 (2019).
10. R. R. Isberg, T. J. O'Connor, M. Heidtman, The *Legionella pneumophila* replication vacuole: Making a cosy niche inside host cells. *Nat. Rev. Microbiol.* **7**, 13–24 (2009).
11. E. Haenssler, V. Ramabhadran, C. S. Murphy, M. I. Heidtman, R. R. Isberg, Endoplasmic reticulum tubule protein reticulon 4 associates with the *Legionella pneumophila* vacuole and with translocated substrate Ceg9. *Infect. Immun.* **83**, 3479–3489 (2015).
12. J. C. Kagan, C. R. Roy, *Legionella* phagosomes intercept vesicular traffic from endoplasmic reticulum exit sites. *Nat. Cell Biol.* **4**, 945–954 (2002).
13. M. S. Swanson, R. R. Isberg, Association of *Legionella pneumophila* with the macrophage endoplasmic reticulum. *Infect. Immun.* **63**, 3609–3620 (1995).
14. L. G. Tilney, O. S. Harb, P. S. Connelly, C. G. Robinson, C. R. Roy, How the parasitic bacterium *Legionella pneumophila* modifies its phagosome and transforms it into rough ER: Implications for conversion of plasma membrane to the ER membrane. *J. Cell Sci.* **114**, 4637–4650 (2001).
15. T. J. O'Connor, D. Boyd, M. S. Dorer, R. R. Isberg, Aggravating genetic interactions allow a solution to redundancy in a bacterial pathogen. *Science* **338**, 1440–1444 (2012).
16. Y. Liu *et al.*, Serine-ubiquitination regulates Golgi morphology and the secretory pathway upon *Legionella* infection. *Cell Death Differ.* **28**, 2957–2969 (2021).
17. A. Akturk *et al.*, Mechanism of phosphoribosyl-ubiquitination mediated by a single *Legionella* effector. *Nature* **557**, 729–733 (2018).
18. Y. Dong *et al.*, Structural basis of ubiquitin modification by the *Legionella* effector SdeA. *Nature* **557**, 674–678 (2018).
19. S. Kalayil *et al.*, Insights into catalysis and function of phosphoribosyl-linked serine ubiquitination. *Nature* **557**, 734–738 (2018).
20. Y. Wang *et al.*, Structural insights into non-canonical ubiquitination catalyzed by SidE. *Cell* **173**, 1231–1243.e1216 (2018).
21. J. Qiu *et al.*, Ubiquitination independent of E1 and E2 enzymes by bacterial effectors. *Nature* **533**, 120–124 (2016).
22. K. M. Kotewicz *et al.*, A single *Legionella* effector catalyzes a multistep ubiquitination pathway to rearrange tubular endoplasmic reticulum for replication. *Cell Host Microbe.* **21**, 169–181 (2017).
23. S. Bhogaraju *et al.*, Phosphoribosylation of ubiquitin promotes serine ubiquitination and impairs conventional ubiquitination. *Cell* **167**, 1636–1649.e1613 (2016).
24. D. Shin *et al.*, Regulation of phosphoribosyl-linked serine ubiquitination by deubiquitinases DupA and DupB. *Mol. Cell* **77**, 164–179.e166 (2020).
25. M. Wan *et al.*, Deubiquitination of phosphoribosyl-ubiquitin conjugates by phosphodiesterase-domain-containing *Legionella* effectors. *Proc. Natl. Acad. Sci. U.S.A.* **116**, 23518–23526 (2019).
26. K. C. Jeong, J. A. Sexton, J. P. Vogel, Spatiotemporal regulation of a *Legionella pneumophila* T4SS substrate by the metaeffector SidJ. *PLoS Pathog.* **11**, e1004695 (2015).
27. J. Qiu *et al.*, A unique deubiquitinase that deconjugates phosphoribosyl-linked protein ubiquitination. *Cell Res.* **27**, 865–881 (2017).
28. S. Bhogaraju *et al.*, Inhibition of bacterial ubiquitin ligases by SidJ-calmodulin catalysed glutamylation. *Nature* **572**, 382–386 (2019).
29. J. C. Havey, C. R. Roy, Toxicity and SidJ-mediated suppression of toxicity require distinct regions in the SidE family of *Legionella pneumophila* effectors. *Infect. Immun.* **83**, 3506–3514 (2015).
30. R. K. Laguna, E. A. Creasey, Z. Li, N. Valtz, R. R. Isberg, A *Legionella pneumophila*-translocated substrate that is required for growth within macrophages and protection from host cell death. *Proc. Natl. Acad. Sci. U.S.A.* **103**, 18745–18750 (2006).
31. E. A. Creasey, R. R. Isberg, The protein SdhA maintains the integrity of the *Legionella*-containing vacuole. *Proc. Natl. Acad. Sci. U.S.A.* **109**, 3481–3486 (2012).
32. W. Y. Choi *et al.*, SdhA blocks disruption of the *Legionella*-containing vacuole by hijacking the OCRL phosphatase. *Cell Rep.* **37**, 109894 (2021).
33. S. Sharma, A. Skowronek, K. S. Erdmann, The role of the Lowe syndrome protein OCRL in the endocytic pathway. *Biol. Chem.* **396**, 1293–1300 (2015).
34. M. A. De Matteis, L. Staiano, F. Emma, O. Devuyst, The 5-phosphatase OCRL in lowe syndrome and dent disease 2. *Nat. Rev. Nephrol.* **13**, 455–470 (2017).

35. D. M. Pilla *et al.*, Guanylate binding proteins promote caspase-11-dependent pyroptosis in response to cytoplasmic LPS. *Proc. Natl. Acad. Sci. U.S.A.* **111**, 6046–6051 (2014).
36. B. C. Liu *et al.*, Constitutive interferon maintains GBP expression required for release of bacterial components upstream of pyroptosis and anti-DNA responses. *Cell Rep.* **24**, 155–168.e155 (2018).
37. I. S. Anand, W. Choi, R. R. Isberg, Components of the endocytic and recycling trafficking pathways interfere with the integrity of the *Legionella*-containing vacuole. *Cell Microbiol.* **22**, e13151 (2020).
38. M. N. Seaman, Cargo-selective endosomal sorting for retrieval to the Golgi requires retromer. *J. Cell Biol.* **165**, 111–122 (2004).
39. C. Burd, P. J. Cullen, Retromer: A master conductor of endosome sorting. *Cold Spring Harb. Perspect. Biol.* **6**, a016774 (2014).
40. I. Finsel *et al.*, The *Legionella* effector RidL inhibits retrograde trafficking to promote intracellular replication. *Cell Host Microbe* **14**, 38–50 (2013).
41. K. Barlocher *et al.*, Structural insights into *Legionella* RidL-Vps29 retromer subunit interaction reveal displacement of the regulator TBC1D5. *Nat. Commun.* **8**, 1543 (2017).
42. K. H. Berger, R. R. Isberg, Two distinct defects in intracellular growth complemented by a single genetic locus in *Legionella pneumophila*. *Mol. Microbiol.* **7**, 7–19 (1993).
43. J. M. Park, S. Ghosh, T. J. O'Connor, Combinatorial selection in amoebal hosts drives the evolution of the human pathogen *Legionella pneumophila*. *Nat. Microbiol.* **5**, 599–609 (2020).
44. E. Geisinger *et al.*, Antibiotic susceptibility signatures identify potential antimicrobial targets in the *Acinetobacter baumannii* cell envelope. *Nat. Commun.* **11**, 4522 (2020).
45. K. M. McCoy, M. L. Antonio, T. van Opijnen, MAGenTA: A galaxy implemented tool for complete Tn-Seq analysis and data visualization. *Bioinformatics* **33**, 2781–2783 (2017).
46. T. van Opijnen, K. L. Bodi, A. Camilli, Tn-seq: High-throughput parallel sequencing for fitness and genetic interaction studies in microorganisms. *Nat. Methods* **6**, 767–772 (2009).
47. J. J. Merriam, R. Mathur, R. Maxfield-Boumil, R. R. Isberg, Analysis of the *Legionella pneumophila* flil gene: Intracellular growth of a defined mutant defective for flagellum biosynthesis. *Infect. Immun.* **65**, 2497–2501 (1997).
48. A. D. Hempstead, R. R. Isberg, Inhibition of host cell translation elongation by *Legionella pneumophila* blocks the host cell unfolded protein response. *Proc. Natl. Acad. Sci. U.S.A.* **112**, E6790–E6797 (2015).
49. V. P. Losick, E. Haenssler, M. Y. Moy, R. R. Isberg, LnaB: A *Legionella pneumophila* activator of NF-kappaB. *Cell Microbiol.* **12**, 1083–1097 (2010).
50. J. Schindelin *et al.*, Fiji: An open-source platform for biological-image analysis. *Nat. Methods* **9**, 676–682 (2012).
51. K. C. Barry, N. T. Ingolia, R. E. Vance, Global analysis of gene expression reveals mRNA superinduction is required for the inducible immune response to a bacterial pathogen. *Elife* **6**, e22707 (2017).
52. I. Derre, R. R. Isberg, Macrophages from mice with the restrictive Lgn1 allele exhibit multifactorial resistance to *Legionella pneumophila*. *Infect. Immun.* **72**, 6221–6229 (2004).
53. J. P. Bardill, J. L. Miller, J. P. Vogel, IcmS-dependent translocation of SdeA into macrophages by the *Legionella pneumophila* type IV secretion system. *Mol. Microbiol.* **56**, 90–103 (2005).
54. D. J. Lampe, M. E. Churchill, H. M. Robertson, A purified mariner transposase is sufficient to mediate transposition in vitro. *EMBO J.* **15**, 5470–5479 (1996).
55. B. Byrne, M. S. Swanson, Expression of *Legionella pneumophila* virulence traits in response to growth conditions. *Infect. Immun.* **66**, 3029–3034 (1998).
56. G. M. Conover, I. Derre, J. P. Vogel, R. R. Isberg, The *Legionella pneumophila* LidA protein: A translocated substrate of the Dot/Icm system associated with maintenance of bacterial integrity. *Mol. Microbiol.* **48**, 305–321 (2003).
57. T. J. O'Connor, Y. Adepoju, D. Boyd, R. R. Isberg, Minimization of the *Legionella pneumophila* genome reveals chromosomal regions involved in host range expansion. *Proc. Natl. Acad. Sci. U.S.A.* **108**, 14733–14740 (2011).
58. S. R. Shames *et al.*, Multiple *Legionella pneumophila* effector virulence phenotypes revealed through high-throughput analysis of targeted mutant libraries. *Proc. Natl. Acad. Sci. U.S.A.* **114**, E10446–E10454 (2017).
59. D. T. Isaac, R. K. Laguna, N. Valtz, R. R. Isberg, MavN is a *Legionella pneumophila* vacuole-associated protein required for efficient iron acquisition during intracellular growth. *Proc. Natl. Acad. Sci. U.S.A.* **112**, E5208–E5217 (2015).
60. B. Iglewicz, D. C. Hoaglin, *How to Detect and Handle Outliers, ASQC Basic References in Quality Control* (ASQC Quality Press, Milwaukee, Wis, 1993), p. 87.
61. Y. Benjamini, A. M. Krieger, D. Yekutieli, Adaptive linear step-up procedures that control the false discovery rate. *Biometrika* **93**, 491–507 (2006).
62. M. Romano-Moreno *et al.*, Molecular mechanism for the subversion of the retromer coat by the *Legionella* effector RidL. *Proc. Natl. Acad. Sci. U.S.A.* **114**, E11151–E11160 (2017).
63. J. Lippmann *et al.*, Bacterial internalization, localization, and effectors shape the epithelial immune response during *Shigella flexneri* infection. *Infect. Immun.* **83**, 3624–3637 (2015).
64. K. McGourty *et al.*, *Salmonella* inhibits retrograde trafficking of mannose-6-phosphate receptors and lysosome function. *Science* **338**, 963–967 (2012).
65. A. H. Gaspar, M. P. Machner, VipD is a Rab5-activated phospholipase A1 that protects *Legionella pneumophila* from endosomal fusion. *Proc. Natl. Acad. Sci. U.S.A.* **111**, 4560–4565 (2014).
66. B. Ku *et al.*, VipD of *Legionella pneumophila* targets activated Rab5 and Rab22 to interfere with endosomal trafficking in macrophages. *PLoS Pathog.* **8**, e1003082 (2012).
67. M. Mari *et al.*, SNX1 defines an early endosomal recycling exit for sortilin and mannose 6-phosphate receptors. *Traffic* **9**, 380–393 (2008).
68. J. A. Solinger, H. O. Rashid, C. Prescianotto-Baschong, A. Spang, FERARI is required for Rab11-dependent endocytic recycling. *Nat. Cell Biol.* **22**, 213–224 (2020).
69. I. Anand, W. Choi, R. R. Isberg, The vacuole guard hypothesis: How intravacuolar pathogens fight to maintain the integrity of their beloved home. *Curr. Opin. Microbiol.* **54**, 51–58 (2020).
70. C. R. Beuzon *et al.*, *Salmonella* maintains the integrity of its intracellular vacuole through the action of SifA. *EMBO J.* **19**, 3235–3249 (2000).
71. C. A. Elwell *et al.*, *Chlamydia trachomatis* co-opts GBF1 and CERT to acquire host sphingomyelin for distinct roles during intracellular development. *PLoS Pathog.* **7**, e1002198 (2011).
72. C. van Ooij *et al.*, Host cell-derived sphingolipids are required for the intracellular growth of *Chlamydia trachomatis*. *Cell Microbiol.* **2**, 627–637 (2000).
73. N. Mellouk *et al.*, *Shigella* subverts the host recycling compartment to rupture its vacuole. *Cell Host Microbe* **16**, 517–530 (2014).
74. J. Ruiz-Albert *et al.*, Complementary activities of SseJ and SifA regulate dynamics of the *Salmonella typhimurium* vacuolar membrane. *Mol. Microbiol.* **44**, 645–661 (2002).
75. X. Li, D. E. Anderson, Y. Y. Chang, M. Jarnik, M. P. Machner, VpdC is a ubiquitin-activated phospholipase effector that regulates *Legionella* vacuole expansion during infection. *Proc. Natl. Acad. Sci. U.S.A.* **119**, e2209149119 (2022).
76. M. Zhang *et al.*, Members of the *Legionella pneumophila* Sde family target tyrosine residues for phosphoribosyl-linked ubiquitination. *RSC Chem. Biol.* **2**, 1509–1519 (2021).
77. M. Zhang, S. Kim, R. R. Isberg, The Sde phosphoribosyl-linked ubiquitin transferases exploit reticulons to protect the integrity of the Legionella-containing vacuole. bioRxiv [Preprint] (2023). 10.1101/2023.06.27.546723. Accessed 27 June 2023.
78. Y. Abu Kwaik, The phagosome containing *Legionella pneumophila* within the protozoan *Hartmannella vermiformis* is surrounded by the rough endoplasmic reticulum. *Appl. Environ. Microbiol.* **62**, 2022–2028 (1996).
79. Y. Liu, Z. Q. Luo, The *Legionella pneumophila* effector SidJ is required for efficient recruitment of endoplasmic reticulum proteins to the bacterial phagosome. *Infect. Immun.* **75**, 592–603 (2007).